ASTM INTERNATIONAL

Journal of Testing and Evaluation

Christiane Raab[1] and Manfred N. Partl[2]

DOI: 10.1520/JTE20190165

Mechanical Evaluation of Concrete Bridge Deck Pavement Systems

Copyright by ASTM Int'l (all rights reserved); Thu Oct 17 07:09:21 EDT 2019
Downloaded/printed by
Library for the Research Institutes within the ETH Domain Eawag (Library for the Research Institutes within the ETH Domain Eawag) pursuant to License Agreement. No fur

Journal of Testing and Evaluation

doi:10.1520/JTE20190165 available online at www.astm.org

Christiane Raab[1] and Manfred N. Partl[2]

Mechanical Evaluation of Concrete Bridge Deck Pavement Systems

Reference

C. Raab and M. N. Partl, "Mechanical Evaluation of Concrete Bridge Deck Pavement Systems," *Journal of Testing and Evaluation* https://doi.org/10.1520/JTE20190165

ABSTRACT

Asphalt pavement systems for concrete bridge decks must not only comply with requirements from traffic and environmental exposure but also provide protection of the concrete structures against corrosive attacks from water or deicing agents. These multifunctional expectations are major challenges not only from the material side but also from the experimental side as to the evaluation of the right test methods for assessing the mechanical behavior of the whole multilayer pavement system. In this article, the results of a research project comparing different asphalt pavement systems for alpine regions are presented. These systems consist of hot rolled and mastic asphalt for wearing and protection layers placed on waterproofing systems with polymer bitumen sheets, liquid polymer, and mastic asphalt. The study revealed both the mechanical differences between the different systems and the weaknesses or strengths of different mechanical tests, clearly demonstrating that one has to be careful in interpreting seemingly contradictory results of different test methods. In particular, it was interesting to see that the rutting assessment for some systems differs between cyclic compression tests and rutting tests conducted with a model mobile load simulator.

Keywords

bridge deck pavement systems, mechanical evaluation, cyclic compression test, interlayer bonding test, rutting test, dynamic creep test

Manuscript received December 7, 2018; accepted for publication September 13, 2019; published online October 15, 2019.

[1] Department of Road Engineering, Empa Laboratory for Road Engineering/Sealing Component, Swiss Federal Laboratories for Material Science and Technology, Ueberlandstr. 129, Empa, Duebendorf, Switzerland (Corresponding author), e-mail: christiane.raab@empa.ch, https://orcid.org/0000-0003-3381-0184

[2] Department of Road Engineering, Empa Laboratory for Road Engineering/Sealing Component, Swiss Federal Laboratories for Material Science and Technology, Ueberlandstr. 129, Empa, Duebendorf, Switzerland

Introduction

Concrete bridge decks need protection from water and de-icing agents and a pavement structure that is particularly resistant to permanent deformation due to extremely canalized traffic and special climatic conditions due to extended sun exposure. Although a lack of protection or damage protection layers may cause corrosion and serious long-term failure of the supporting structure, large permanent deformations may promote ice formation

Copyright by ASTM Int'l (all rights reserved); Thu Oct 17 07:09:21 EDT 2019
Copyright © 2019 by ASTM International, 100 Barr Harbor Drive, PO Box C700, West Conshohocken, PA 19428-2959
Downloaded/printed by
Library for the Research Institutes within the ETH Domain Eawag (Library for the Research Institutes within the ETH Domain Eawag) pursuant to License Agreement. No fur

and aquaplaning within the rutted wheel paths, thus creating safety risks for drivers. Moreover, rutting is often the result of the loss of bond between the individual pavement layers and thus fosters structural damage from interlayer water infiltration. Mechanical resistant bridge deck pavement systems are needed, particularly in cases where special environmental requirements such as noise reduction have to be taken into consideration, and though new pavement systems and products for bridges have been developed, their applicability and durability have yet to be proven. In Switzerland, different systems that combine soft bituminous layers and classical stiff layers are used for the insulation of concrete bridge decks. Recently, new pavements with improved noise reduction properties, such as semidense low-noise asphalt (SDA), have attracted a lot of interest.

A detailed comparative description of the systems and materials used mostly at a European level can be found in a position paper by the European Asphalt Pavement Association.[1] It covers pavements not only laid on top of concrete but also on steel bridge decks.[2] However, research and recommendations focus mainly on the performance of single functional layers. In fact, numerous literature is available, discussing the mechanical performance of individual layers relying on considerable number of different tests for determining stability and mechanical resistance of the individual pavement layers.[3–5] Nevertheless, their suitability for assessing durability and function of the whole bridge deck pavement system under load, with respect to interlayer bonding and mechanical dynamic behavior such as rutting, has been scarcely evaluated so far.[6,7]

Hence, a research project to evaluate the performance of typical Swiss bridge deck pavement systems using different test methods was launched; additionally, the suitability of noise-reducing SDA for Swiss conditions was studied. In this context, the suitability of the test methods for assessment of the properties of the whole system should also be investigated. Special attention should be given regarding the influence of waterproofing on the permanent deformation of the systems. As for the test methods, permanent deformation under cyclic vertical compression, rolling wheel loads applied with a model traffic load simulator, and dynamic creep under quasistatic confined conditions were considered. Moreover, the bonding between the layers of the pavement system was investigated using interlayer shear tests.

Experimental Procedure

The mechanical and structural resistance of different bridge deck pavement systems was evaluated according Swiss standard SN 640 450, *Abdichtungssysteme und bitumenhaltige Schichten auf Betonbrücken*.[8] The combinations of bituminous layers with waterproofing membranes or polymer coatings are shown in **Table 1**. All systems were constructed and placed on similarly fabricated and conditioned standard concrete bridge deck plates with dimensions of 2,600 by 1,600 mm. All concrete surfaces were dry cleaned (brushing or air-blasting). Systems 1–6 were also sandblasted. The bituminous waterproofing sheets (Polymer Bitumen Dichtungsbahn [PBD]) of Systems 2, 3, and 4 were polymer modified with styrene-butadiene-styrene (SBS) elastomer and, in the case of System 1, with atactic polypropylene (APP) plastomer. For Systems 5 and 6, alternatively, liquid polyurethane polymer (FLK PU) and liquid polymer acrylic glass (FLK PMMA) were used for waterproofing. The design thickness of the waterproofing layers ranged between 3 and 5 mm. For Systems 7 and 8, the waterproofing design consisted of 28-mm-thick mastic asphalt (MA) 8, as specified in Swiss Standard SN 640 441a-NA, *Asphaltmischgut, Mischgutanforderungen – Teil 6: Gussasphalt*,[9] and applied as a so-called floating application, using oil paper to prevent MA8 from boding to the concrete surface. Floating applications have been successfully used on some bridges in Switzerland, provided that all

TABLE 1
Material types and structures of the bridge deck systems

System No.	1	2	3	4	5	6	7	8
Surface layer	MA 11	MA 11	SDA 8	MA 8	MA 11	MA 11	MA 8	SDA 8
Binder layer	…	…	MA 11	MA 11	…	…	…	…
Protection layer	MA 16	MA 16	MA 16	MA 16	MA 16	MA 16	MA 11	MA 11
Waterproofing	PBD APP	PBD SBS	PBD SBS	PBD SBS	FLK PU	FLK PMMA	MA 8 on oil paper	MA 8 on oil paper

Copyright by ASTM Int'l (all rights reserved); Thu Oct 17 07:09:21 EDT 2019
Downloaded/printed by
Library for the Research Institutes within the ETH Domain Eawag (Library for the Research Institutes within the ETH Domain Eawag) pursuant to License Agreement. No fur

TABLE 2
Test used for the different systems

Test Method	Tested System
Interlayer bond test (LPDS)	Systems 1–8
Cyclic compression test (CCT)	Systems 1–8
Rutting test (MMLS-RT)	Systems 1, 2, 5, 6
Dynamic creep test (DCT)	Systems 1, 2, 5, 6

lateral joints were carefully sealed and constructed. This system has advantages in terms of avoiding blistering under the bridge deck pavements, reduction of thermal movement restraints in the pavement, as well as comparatively easy inspection and joint sealing repair. All protection layers with design thicknesses between 37 and 47 mm were made of MA 16 or MA 11. In the case of Systems 3 and 4, a 37-mm-thick binder layer of MA 11 was applied. The surface layers consisted of MA 11 or MA 8 with design thicknesses of 38 and 30 mm, respectively. For Systems 3 and 8, an SDA surface layer constructed according to the Swiss prestandard SNR 640 436, *Semidichtes Mischgut und Deckschichten SDA, Festlegungen, Anforderungen, Konzeption und Ausführung*,[10] with a design thickness of 30 mm. The SDA had a gap-graded mineral aggregate curve, a binder content of 6 %, and an air void content up to 16 vol%. The waterproofing and MA layers were placed manually at ambient temperature. The SDA 8 for Systems 3 and 8 was compacted with a hand roller. More details on waterproofing materials and asphalt mixtures are given in the research report by Raab and Partl.[11]

The four different test methods used to evaluate the mechanical resistance are listed in **Table 2**. The interlayer bond test (Layer-Parallel Direct Shear [LPDS]) and cyclic compression test (CCT) were used for all eight systems. However, the LPDS was only performed at the individual interlayers of the bridge deck pavement systems and not at the interface to the concrete bridge deck. In the case of Systems 7 and 8, the obvious reason was their floating application. In the other cases, the diameter of the cylindrical specimen was considered too small to capture the roughness of the concrete bridge deck in a representative way for interlayer shear testing. In contrast, all systems could be tested in the CCT, including the upper part of the concrete bridge deck, because this is a homogeneous test that focuses on the overall vertical deformation of the system without the expected marginal influence from the bond between the pavement system and the bridge deck concrete. The only tests considered to provide some indication of the influence of the concrete roughness on the behavior of the bridge deck pavement systems were the rutting test (Model Mobile Load Simulator Rutting Test [MMLS-RT]) and the dynamic creep test (DCT). Because MA 8, 11, and 16 as well as the waterproofing layers are nonporous layers, ruts were expected to occur from inhomogeneous material flow along a dominant sliding zone that might activate shear stresses on the concrete surface. Similar effects could also occur in the case of DCT, in spite of the small diameter of these specimens. Thus, MMLS-RT and DCT were performed on the four directly comparable nonfloating Systems 1, 2, 5, and 6 with different waterproofing and similar total thicknesses, i.e., without binder layer.

Interlayer Bond Testing

The LPDS test device (**fig. 1**) was used to investigate quasistatic interlayer bonding strength of nominal 150-mm cylindrical specimens based on the equipment by Leutner[12] but was modified by Empa to test specimens with a larger range in diameter and underdefined pneumatic clamping, as described by Raab, Partl, and El Halim.[13]

All interlayers of a system were tested until failure, calculating the mean value of shear force and nominal failure stress from six replicas each. Because the diameter of all specimens was the same, only the shear forces are discussed below. The specimens were conditioned for 8 h at 20°C and tested at that temperature with a loading rate of 50 mm/min. **Figure 2** presents the maximum shear force results for the different interlayers: MA on MA, SDA on MA, and MA on waterproofing. **Figure 3** depicts the mean force/stress-deformation curves for all four systems with different waterproofing. The error bars in **figures 2** and **3** denote the standard deviations.

Copyright by ASTM Int'l (all rights reserved); Thu Oct 17 07:09:21 EDT 2019
Downloaded/printed by
Library for the Research Institutes within the ETH Domain Eawag (Library for the Research Institutes within the ETH Domain Eawag) pursuant to License Agreement. No fur

FIG. 1

LPDS test device with pneumatic clamps.

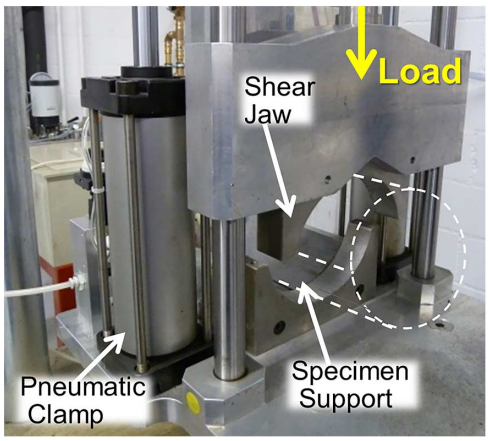

FIG. 2

Interlayer shear bonding strength at 20°C between the layers of all systems (including system numbers).

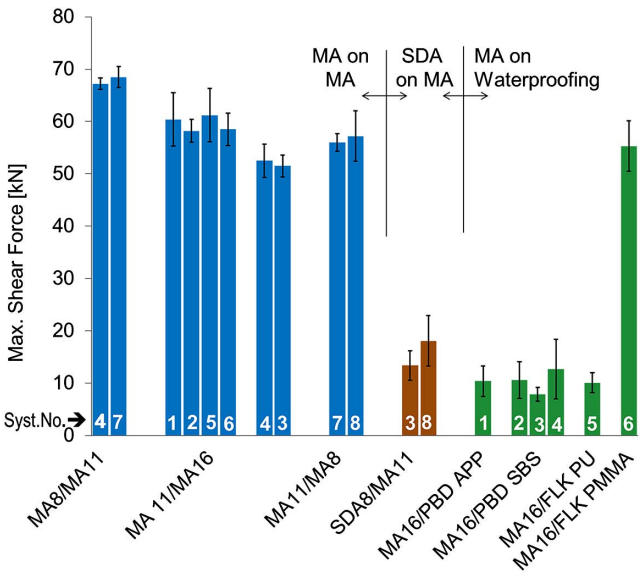

The force/stress-deformation curves in figure 3*A* and 3*B* show a very good interlayer shear bonding strength of about 60 kN, or 3.5 MPa, between the surface and protection layers of Systems 1 and 2 (MA 11/MA 16), whereas the bonding strength value between the protection layer and waterproofing layer is only about 10 kN, i.e., significantly lower. Moreover, the slope for the PBD APP system is significantly steeper that of the PBD SBS system, which indicates stiffer and clearly less ductile behavior.

From figure 2 shows that the mean shear bonding strength between the binder and protection layers (MA 11/MA 16) is similar for Systems 3 and 4 but, with mean values toward 50 kN, they are clearly lower than those between the MA 11/MA 16 of Systems 1, 2, 5, and 6. Hence, it cannot be excluded that, in the case of Systems 3 and 4, placing the surface layers may have had a negative influence on the bonding strength between the binder and protection layers. The bond between surface and binder layers is remarkably different. As compared with the surface course MA 8 on MA 11 of System 4, with a mean strength of 67.2 kN, the SDA 8 on MA 11 of System 3 reaches only 13.4 kN. This is a clear sign of weakness for systems with SDA, which is due to its significantly higher

Copyright by ASTM Int'l (all rights reserved); Thu Oct 17 07:09:21 EDT 2019
Downloaded/printed by
Library for the Research Institutes within the ETH Domain Eawag (Library for the Research Institutes within the ETH Domain Eawag) pursuant to License Agreement. No fur

FIG. 3 Interlayer shear forces versus deformation for the pavement systems with different waterproofing: (*A*) PBD APP, (*B*) PBD SBB, (*C*) FLK PU, (*D*) FLK PMMA.

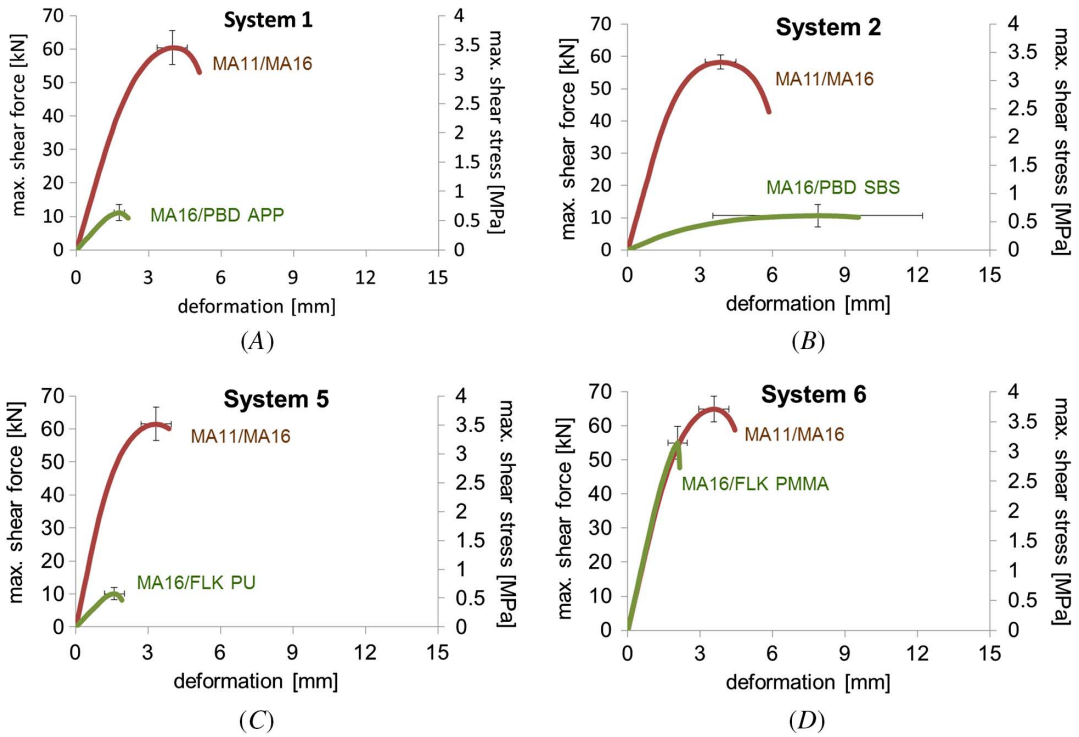

air voids, providing fewer contact areas for transferring shear stresses. As for the bond to the waterproofing, again, the mean shear strength between protection layer MA 16 and PBD SBS is significantly low. It reaches 7.9 and 12.7 kN for Systems 3 and 4, respectively, which is in the same order of magnitude as that of System 2. This can be explained by the fact that the PBD contains a comparatively high amount of SBS-modified binder that, according to its viscosity, acts like a lubricant in this case.

According to **figures 2** and **3C**, the interlayer shear bond between surface and protection layers MA 11/MA 16 of Systems 5 and 6 are both close to 60 kN. On the other hand, huge differences exist between the protection and waterproofing layers, which displaying only 10.1 kN bonding strength in the case of System 5 with FLK PU and 55.3 kN for System 6 with FLK PMMA. Moreover, although the bond between the protection layer and the waterproofing for System 5 is of comparable stiffness to System 1, the slope of the curve for System 6 is significantly higher and almost equal to MA 11/MA 16.

The bonding strengths between the surface and the layer below of Systems 7 and 8 are 68.6 and 18.1 kN, respectively, which is similar to those of Systems 3 and 4. Again, the bond of the MA 8 of System 7 was clearly superior to the SDA 8 of System 8. The interlayer bond between the protection and waterproofing layers (MA 11/MA 8) of both systems reaches similar strength values of around 57 kN.

Figure 2 demonstrates that shear bonding between undamaged MA layers is clearly unproblematic, reaching strength values in the order of 60 kN at 20°C. Apparently, for MA, there is a tendency that finer layers on coarser layers (e.g., MA 8/MA 11) give better interlayer strength than coarser layer on finer layers (MA 11/MA 8). It also appears that the interlayer strength between finer MA layers (MA 8/MA 11) is slightly higher than that between comparable coarser layers (MA 11/MA 16). However, for SDA placed on MS (SDA/MA) of Systems 3 and 8, the situation appears totally different. These systems did not meet the bonding strength of 15 kN between surface and binder course as required by Swiss standards (SN 640 430c, *Walzasphalt, Konzeption, Ausführung und Anforderung*

Copyright by ASTM Int'l (all rights reserved); Thu Oct 17 07:09:21 EDT 2019
Downloaded/printed by
Library for the Research Institutes within the ETH Domain Eawag (Library for the Research Institutes within the ETH Domain Eawag) pursuant to License Agreement. No fur

an die eingebauten Schichten). Also quite poor is the interlayer bonding between the MA protection layers and the APP and SBS-modified waterproofing of Systems 1–4, as well as the liquid polyurethane polymer FLK PU of System 5. However, in the case of System 6, a bond that was five times stronger between MA and FLK PMMA was achieved.

CCT

The CCT is described both in European and German standards (Europe: EN 12697-25, *Bituminous Mixtures—Test Methods for Hot Mix Asphalt—Part 25: Cyclic Compression Test*,[14]; Germany: TP asphalt-StB part 25 B1, *Einaxialer Druckschwellversuch - Bestimmung des Verformungsverhaltens von Walzasphalt bei Wärme*[15]). In this study, the German test was used as a guideline because it allows more homogeneous loading due to the larger loading plate and therefore a more uniform loading of the waterproofing layer at the bottom of the multilayered specimens as shown in **figure 4**. Specimens were cored from each system, including 15 mm of the bridge deck concrete. Axial haversine-pulse pressure loading cycles with rest periods were applied according to **Table 3**, which also presents other relevant test parameters. For each system, three specimens were loaded with 10,000 cycles. The nominal strain limit value was 4 %. The resulting cyclic compression creep curves for the different systems in **figure 5** display the mean values of the cumulative nominal axial strain, in a percentage of the original specimen height, versus the number of loading cycles. The error bars denote the maximum and minimum values out of three replicas.

The dynamic compression curves quite clearly follow a power law approach in the form of $y = a\ N^q$. They display relatively large deformations for Systems 1–8, especially System 3, for which the nominal permanent strain limit of 4 % is reached after only a few hundred cycles and which has a very low resistance against permanent deformation in the laterally unconfined CCT at 50°C. The best creep resistance with 8,000 load cycles until a 4 % nominal permanent strain is achieved for System 7 and followed by System 8 with approximately 4,000 load cycles at 4 % strain. For both systems, the difference between the maximum and minimum values is also small,

FIG. 4

Test setup for the CCT. LVDT, linear variable differential transformer.

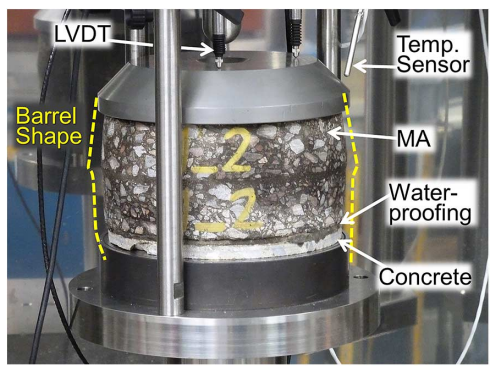

TABLE 3

Testing parameters for the CCT

Parameter	Value
Testing temperature	50 ± 0.3°C
Specimen diameter	148 ± 5 mm
Duration of load cycle	1.7 s
Duration of haversine load pulse	0.2 s
Duration of rest period	1.5 s
Upper compression stress	0.2 MPa
Lower compression stress	0.025 MPa

Copyright by ASTM Int'l (all rights reserved); Thu Oct 17 07:09:21 EDT 2019
Downloaded/printed by
Library for the Research Institutes within the ETH Domain Eawag (Library for the Research Institutes within the ETH Domain Eawag) pursuant to License Agreement. No fur

FIG. 5

CCT results at 50°C for all systems, showing scatter bars for minimum and maximum values together as well as the 4 % limit that German standards consider critical.

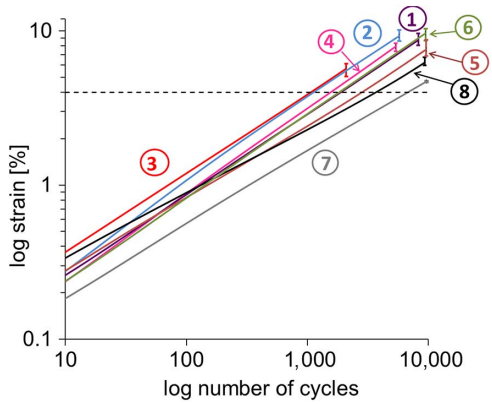

particularly in the case of System 7. System 5 reaches 4 % permanent strain after 3,000 load cycles, whereas the rest of the systems required less than 2,000 load cycles. **Figure 5** shows that Systems 7 and 8 produced the smallest and Systems 2 and 4 the highest permanent strain rate and therefore the highest q values in the power law approach. The mean values of the measured layer thicknesses before and after CCT are presented in **Table 4**. From these values, the individual thickness change of the layers after 10,000 cycles was calculated using a power law approach and depicted in **figure 6** for a better comparison. The results reveal that in the case of Systems 1, 2, and 5, with an MA surface course of nominal maximal aggregate size (NMAS) 11 mm, the specimens deform quite uniformly in all asphalt layers, leading to a bulge in the middle. The surface layers of Systems 3, 4, 7, and 8 with NMAS 8 mm showed less deformation, suggesting that in this special case a smaller NMAS was favorable. As compared with the

TABLE 4

Layer thickness before and after CCT (mean values in mm)

System No.	1	2	3	4	5	6	7	8
Surface layer	36.0/33.3	36.0/32.7	36.7/35.3	28.0/27.3	34.2/31.3	35.7/34.0	30.2/29.0	38.7/37.0
Binder layer	…		37.7/35.0	36.0/33.0	…	…	…	…
Protection layer	33.0/30.0	35.8/31.7	34.7/32.0	32.0/29.3	33.0/30.5	34.8/30.2	35.3/34.2	32.7/31.0
Waterproofing	4.8/4.7	4.0/2.8	5.0/3.8	5.2/4.8	4.5/4.3	2.8/2.4	28.8/26.7	30.3/27.7
Total thickness	73.8/68.0	75.8/67.2	114.0/106.2	101.2/94.5	71.7/66.2	73.3/66.6	94.3/89.8	101.7/95.7

FIG. 6

Layer thickness changes of the different systems at 50°C calculated for 10,000 cycles using a power function approach.

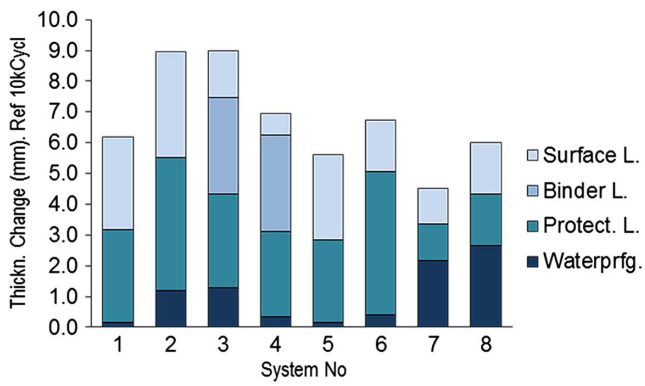

Copyright by ASTM Int'l (all rights reserved); Thu Oct 17 07:09:21 EDT 2019
Downloaded/printed by
Library for the Research Institutes within the ETH Domain Eawag (Library for the Research Institutes within the ETH Domain Eawag) pursuant to License Agreement. No fur

surface layer MA 8, the SDA 8 appeared slightly more deformable, which was probably due to the lack of lateral confinement in the CCT. As for the waterproofing, the contribution of the SBS-modified sheets to the total deformation was clearly higher than it was for System 1 with the APP-modified sheet, whose deformation was comparable to the liquid FLK PU and FLK PMMA waterproofing of Systems 5 and 6. For Systems 7 and 8, the deformation can be found mainly in the waterproofing layer (MA 8). Remember, these two systems were floating applications and could therefore not be tested with the bridge deck concrete because it would cause separating of the oil paper. Therefore, during testing, the waterproofing MA 8 was not hindered in moving laterally at its bottom by the surface roughness of the bridge deck concrete and was therefore less resistant to deformation under compression in the CCT.

Rutting Testing

Rutting tests using MMLS-RT were conducted with model mobile load simulator MMLS3 that was developed by Hugo and Epps.[16] A scaled tire load of 2.1 kN was applied in one trafficking direction with four pneumatic 300-mm wheels that were inflated up to 600 kPa (**fig. 7*A***). The distance between the tires was 1.05 m. The machine (length × width × height = 2.4 × 0.6 × 1.2 m^3) enables about 7,200 load applications per hour, i.e., a speed of 2.6 m/s. This corresponds to a loading frequency of about 4 Hz for a measured tread length of 0.11 m. Testing was performed at 20°C, and up to 0.5-million load passings without lateral wandering of the loading tires on Systems 1, 2, 5, and 6. These systems were selected for studying the effect of the MMLS-RT on the four waterproofing systems: PBD APP, PBD SBS, FLK PU, and FKL PMMA. For each investigated system, two longitudinal rut paths were produced, one on each side of the plate as shown in **figure 7*B***. The mean depth of the three rut profiles (left-middle-right) was calculated and averaged with the values of the fellow rut path as presented in **Table 5**. **Figure 8** presents the rut depth measurements of the individual rut paths together with the corresponding power function regression curves for each system. With these functions, the rut depths after 0.5- and 1-million load passings were calculated (**Table 5**). Because one rut path of System 2 showed an extensive deformation of 20.9 mm already after 34,000 passings, requiring immediate experimental cutoff, the regression curve for this system probably

FIG. 7 (*A*) Model mobile load simulator MMLS3 and (*B*) rut profiles and coring positions on System 5.

(*A*) (*B*)

TABLE 5
Rut depth measured and calculated (average of two rut paths)

Rut Depth (mm)	System 1	System 2	System 5	System 6
500,000 cycles (measured)	15.9	13.7 (for profile 1) >20.9 (for profile 2)	14.6	10.9
500,000 passings (calculated)	18.0	18.5 (20.3)	17.1	13.7
1,000,000 passings (calculated)	20.1	26.5 (29.2)	26.9	18.1

Copyright by ASTM Int'l (all rights reserved); Thu Oct 17 07:09:21 EDT 2019
Downloaded/printed by
Library for the Research Institutes within the ETH Domain Eawag (Library for the Research Institutes within the ETH Domain Eawag) pursuant to License Agreement. No fur

FIG. 8

Rutting test results for Systems 1, 2, 5, and 6.

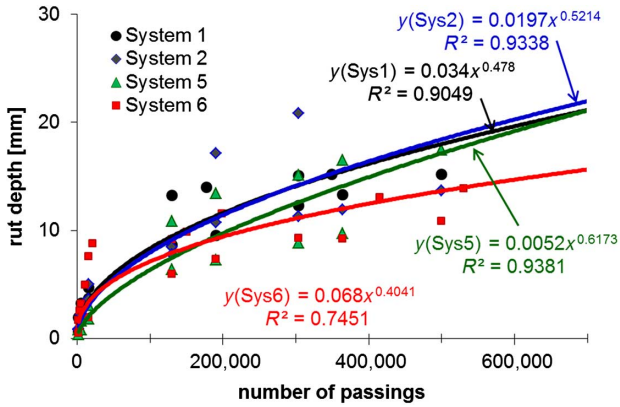

underestimates the calculated deformations for high numbers of load passings by about 10 % as compared with the figures in brackets, calculated from a regression with extrapolated missing values for the cutoff test.

According to figure 8 and the rut depth data shown in Table 5, System 6 shows the smallest rutting and therefore the greatest resistance against permanent deformation. All other systems behave quite similarly. System 2, with the deepest ruts, shows very distinct differences between the two rut profiles. These results are in accordance with the results found in the CCT (fig. 6), in which System 2 with the SBS-modified waterproofing was also the system with the most deformation as compared with Systems 1, 3, and 6, which performed similarly in the CTT. However, when comparing the CCT and rutting test results of System 6, some discrepancy exists. Although System 6 as whole was quite deformable in the 50°C CCT, it was clearly the least deformable in the MMLS-RT at 20°C. However, figure 8 shows that System 6, compared with Systems 1, 2, and 5, suffered the least deformation in the surface course alone. This coincides well with the high rutting resistance of System 6 in the MMLS-RT and suggests that the MMLS-RT at 20°C primarily had an effect on the deformation behavior of the upper layers but was not very effective on the lower layers. This may also explain why, from the MMLS-RT at 20°C, no clear influence of the waterproofing systems could be detected.

After MMLS-RT, six cores were taken both within and outside the ruts and the interlayer shear strength was determined. The results showed an average increase of interlayer strength under the wheel path between the surface and protection layer MA 11/MA 16 of 2.1 %. As for the interlayer strength between the protection and waterproofing layers, only System 1, with the APP waterproofing sheet, resulted in an average increase by 7.2 %, whereas Systems 2 and 6 produced a decrease by 12.3 and 11.8 %, respectively, and System 5, with FLK PU, had a decrease by 21.8 %. In spite of the fact that these results are not statistically significant, they still suggest that trafficking and traffic-induced vibrations of the structure may weaken the bond between the asphalt protection layers and thin-layered waterproofing systems.

DCT

The DCT was performed without a waterproofing layer to compare the permanent deformation behavior of the different systems with nominally the same surface and protection MA layers, i.e., Systems 1, 2, 5, and 6. Other than the dynamic compression test, it allows testing of a 150-mm cylindrical specimen under quasiconfined conditions due to the fact that the diameter of the axial plunger is only 80 mm, as shown in figure 9*A*. The test is similar to the CCT according the German standard (TP asphalt-StB part 25 A2, *Dynamischer Stempeleindringversuch (DSEV) – Bestimmung des Verformungswiderstandes von Walzasphalten bei Wärme*[17]). Two specimens are used to determine the dynamic creep curve of a system under repeated loading at 50°C, recording the cumulated permanent creep deformation below the center plunger versus the number of

Copyright by ASTM Int'l (all rights reserved); Thu Oct 17 07:09:21 EDT 2019
Downloaded/printed by
Library for the Research Institutes within the ETH Domain Eawag (Library for the Research Institutes within the ETH Domain Eawag) pursuant to License Agreement. No fur

FIG. 9

(*A*) Test setup for the DCT CCT and (*B*) cross section of System 2 after testing. LVDT, linear variable differential transformer.

FIG. 10

DCT results: (*A*) all values for Systems 1, 2, 5, and 6 and (*B*) mean values for all systems.

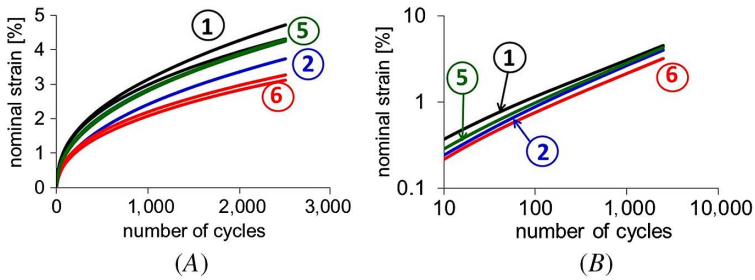

load cycles. The upper stress σ_o is set to 0.35 MPa, and the lower stress σ_u to 0.08 MPa. Results are presented as mean values of two specimens and as nominal strains calculated from the original specimen height and the deformations under the central plunger. An example of these deformations after testing is shown in **figure 9*B***. The DCT was conducted up to 2,500 load cycles for detecting differences in the material (MA). Therefore, the specimens from Systems 1, 2, 5, and 6 were prepared by removing the waterproofing and concrete layers. **Figure 10*A*** shows all test results for Systems 1, 2, 5, and 6, and **figure 10*B*** shows the mean value calculated for Systems 1 and 2 and Systems 5 and 6 in double logarithmic scale, confirming approximately a power function–like creep behavior.

According to the DCT results, Systems 1, 2, and 5 are weaker than System 6, which is the stiffest of all tested systems. These results confirm the MMLS-RT rutting test results, wherein System 6 was also found to have the least rutting, due to its comparatively deformation-resistant surface course and System 2 had the highest rutting due to its comparatively deformable surface layer. The results are not in good agreement with the total deformations measured in the CCT, but they demonstrate that the DCT at 50°C, like the MMLS-RT at 20°C, is primarily effective on the surface layers and therefore not suited for assessing the whole bridge deck pavement system, particularly with respect to the waterproofing. It is interesting to note that in the DCT the scatter for the two specimens taken from System 2 was quite large. This could also be observed in the rutting test, wherein the difference between the two rut profiles was bigger than for all other systems.

Conclusion

This research shows that some testing methods that were originally developed for asphalt concrete systems, such as the CCT, cannot be transferred a priori to bridge deck systems that consist of MA or SDA courses. Both the DCT, with a central plunger at 50°C, and the rutting test (MMLS-RT), with MMLS3 at 20°C, were basically only suitable for testing the upper layers with good agreement in terms of ranking. However, they did not provide information on the deformation behavior of the lower layers, in particular the waterproofing layers. The dynamic compression (CCT) and interlayer shear (LPDS) tests are more advantageous in that respect because they allow the testing of each layer individually. However, it was found that the MMLS-RT weakened the interlayer bond

Copyright by ASTM Int'l (all rights reserved); Thu Oct 17 07:09:21 EDT 2019
Downloaded/printed by
Library for the Research Institutes within the ETH Domain Eawag (Library for the Research Institutes within the ETH Domain Eawag) pursuant to License Agreement. No fur

between the asphalt layers and most of the investigated thin-layered waterproofing systems, suggesting that trafficking and traffic-induced vibrations of the structure must not be neglected and should therefore be a subject of further research.

When comparing stability and deformation of the different systems with the CCT at 50°C, it appeared that MA surface and protection layers with smaller NMAS suffered less permanent deformation. However, as compared with the MA 8 surface courses, the SDA 8 layer appeared more deformable because of its minor stability and should therefore not be favored over MA in terms of mechanical performance. The CCT also showed clearly that thick systems with three bituminous layers on top of a polymer-modified waterproofing membrane should be avoided because of the higher risk of permanent deformations.

As for the waterproofing, the contribution of the SBS-modified sheets to the total deformation in the CTT was clearly higher than it was for System 1 with the APP-modified sheet, whose deformation was comparable to the liquid FLK PU and FLK PMMA polymer waterproofing of Systems 5 and 6.

For the rutting test, Systems 1, 2, 5, and 6 were selected to evaluate the influence of different waterproofing systems (PBD APP, PBD SBS, FLK PU, and FKL PMMA) on the permanent deformation of the system, and therefore it was not possible to give an overall performance ranking for all eight bridge deck systems. Regarding rutting by MMLS-RT at 20°C and the DCT at 50°C, respectively, System 6 seems to have the best properties of the four tested systems. Because it was found that the deformation after rutting was mainly concentrated in the upper layer, both tests appear incapable of evaluating the deformation behavior of the whole system. Therefore, for evaluating and validating the rutting and vibration resistance of a whole bridge deck pavement system, it is necessary to perform testing using in situ full-scale traffic simulators, such as the mobile load simulator MLS10 or heavy vehicle load simulator. For lab testing with MMLS3 or other devices, the layer thicknesses should be reduced.

The interlayer bond at 20°C with LPDS revealed a tendency that, for MA, finer layers on coarser layers (e.g., MA 8/MA 11) produce better interlayer strength than coarser on finer layers (MA 11/MA 8). It also appeared that the interlayer strength between finer MA layers (MA 8/MA 11) was slightly higher than that between comparable coarse layers (MA 11/MA 16). Overall, LPDS showed excellent bonding for all MA layers, with maximum shear forces of more than 60 kN. The bonding property of the SDA layers was considerably lower (12–16 kN) and should be considered critical in reference to the required value of 15 kN identified in Swiss standards. Thus, because of their poor stability and unfavorable shear values, semidense bridge deck systems should be limited to special situations, for example where noise abatement measures are required. The interlayer bond for all thin waterproofing layers displays maximum shear forces between 8 and 12 kN, whereby no difference between APP- and SBS-modified systems was discernible. In contrast to this, the FLK PMMA waterproofing system with a shear force of 55 kN reached the best value among the studied waterproofing layers and can be considered a highly promising system.

References

1. European Asphalt Pavement Association, *Asphalt Pavements on Bridge Decks, EAPA Position Paper* (Brussels, Belgium: European Asphalt Pavement Association, 2013).
2. S. Pouget, C. Sauzéat, H. Di Benedetto, and F. Olard, "Modeling of Viscous Bituminous Wearing Course Materials on Orthotropic Steel Deck," *Materials and Structures* 45, no. 7 (January 2012): 1115–1125. https://doi.org/10.1617/s11527-011-9820-z
3. M. Castro, "Structural Design of Asphalt Pavement on Concrete Bridges," *Canadian Journal of Civil Engineering* 31, no. 4 (August 2004): 695–702. https://doi.org/10.1139/l04-032
4. K. Oba and M. N. Partl, "Non-destructive IR-Thermography for Distress Detection in Asphalt Pavements and Bridge Deck Surfacings," *Road Materials and Pavement Design* 1, no. 4 (2000): 407–418. https://doi.org/10.1080/14680629.2000.12067153
5. B. W. Hailesilassie and M. N. Partl, "Mechanisms of Asphalt Blistering on Concrete Bridges," *Journal of ASTM International* 9, no. 3 (March 2012): 1–16. https://doi.org/10.1520/JAI104135
6. M. Witczak, *Simple Performance Tests: Summary of Recommended Methods and Database, NCHRP Report 547* (Washington, DC: Transportation Research Board, 2005). https://doi.org/10.17226/13949
7. R. C. Eliott and M. Sida, "Performance Testing of Mastic Asphalt for Bridge Surfacing," in *Second Eurasphalt & Eurobitume Congress* (Breukelen, the Netherlands: Foundation Eurasphalt, 2000), 1022–1028.

Copyright by ASTM Int'l (all rights reserved); Thu Oct 17 07:09:21 EDT 2019
Downloaded/printed by
Library for the Research Institutes within the ETH Domain Eawag (Library for the Research Institutes within the ETH Domain Eawag) pursuant to License Agreement. No fur

8. *Abdichtungssysteme und bitumenhaltige Schichten auf Betonbrücken [Waterproofing Systems for Concrete Bridge Decks]*, SN 640 450 (Zurich, Switzerland: Foundation of the Swiss Association of Road and Transport Professionals, approved January 1, 2005).
9. *Asphaltmischgut, Mischgutanforderungen – Teil 6: Gussasphalt [Asphalt Concrete Mixture, Requirements – Part 6:Mastic Asphalt]*, SN 640 441a-NA (Zurich, Switzerland: Foundation of the Swiss Association of Road and Transport Professionals, approved February 1, 2009).
10. *Semidichtes Mischgut und Deckschichten SDA, Festlegungen, Anforderungen, Konzeption und Ausführung [Semi Dense Mixtures and Wearing Courses SDA, Definitions, Requirements, Conception and Construction]*, SNR 640 436 (Zurich, Switzerland: Foundation of the Swiss Association of Road and Transport Professionals, approved September 30, 2015).
11. C. Raab and M. N. Partl, *Forschungspaket Brücken: EP1 - Standfester Gesamtaufbau, Prüfung und Bewertung [Research Package Bridges: EP1-Structural Resistance of the Overall System, Testing and Assessment], Report 1463* (Ittigen, Switzerland: Federal Roads Office, 2014).
12. R. Leutner, "Untersuchungen des Schichtenverbunds beim bituminösen Oberbau [Investigation of the Adhesion of Bituminous Pavements]," *Bitumen* 41, no. 3 (1979): 84–91.
13. C. Raab, M. N. Partl, and O. A. El Halim, "Evaluation of Interlayer Shear Bond Devices for Asphalt Pavements," *Baltic Journal of Road and Bridge Engineering* 4, no. 4 (2009): 186–195. https://doi.org/10.3846/1822-427X.2009.4.186-195
14. *Bituminous Mixtures—Test Methods for Hot Mix Asphalt—Part 25: Cyclic Compression Test*, EN 12697–25 (Brussels, Belgium: European Committee for Standardization, approved April 1, 2005).
15. *Einaxialer Druckschwellversuch - Bestimmung des Verformungsverhaltens von Walzasphalt bei Wärme [Uniaxial Cyclic Compression Test – Determination of Deformation Behavior of Hot Mix Asphalt at Elevated Temperatures]*, TP Asphalt-StB Teil 25 B 1 (Cologne, Germany: Forschungsgesellschaft für Straßen-und Verkehrswesen, 2010).
16. F. Hugo and A. L. Epps, *Significant Findings from Full-Scale Accelerated Pavement Testing, NCHRP Synthesis 325* (Washington, DC: Transportation Research Board, 2004). https://doi.org/10.17226/23380
17. *Dynamischer Stempeleindringversuch (DSEV) – Bestimmung des Verformungswiderstandes von Walzasphalten bei Wärme [Dynamic Indentation Test (DSEV) – Determination of the Deformation Resistance of Hot Mix Asphalt at Elevated Temperatures]*, TP Asphalt-StB Teil 25 A 2 (Cologne, Germany: Forschungsgesellschaft für Straßen-und Verkehrswesen, 2010).

Copyright by ASTM Int'l (all rights reserved); Thu Oct 17 07:09:21 EDT 2019
Downloaded/printed by
Library for the Research Institutes within the ETH Domain Eawag (Library for the Research Institutes within the ETH Domain Eawag) pursuant to License Agreement. No fur